Clim Dyn (2017) 49:1801–1812
DOI 10.1007/s00382-016-3403-1

The Indian winter monsoon and its response to external forcing over the last two and a half centuries

Philipp M. Munz[1] · Andreas Lückge[2] · Michael Siccha[3] · Anna Böll[4] · Sven Forke[5] · Michal Kucera[3] · Hartmut Schulz[1]

Received: 16 December 2015 / Accepted: 14 October 2016 / Published online: 28 October 2016

Abstract The Indian winter monsoon (IWM) is a key component of the seasonally changing monsoon system that affects the densely populated regions of South Asia. Cold winds originating in high northern latitudes provide a link of continental-scale Northern Hemisphere climate to the tropics. Western disturbances associated with the IWM play a critical role for the climate and hydrology in northern India and the western Himalaya region. It is vital to understand the mechanisms and teleconnections that influence IWM variability to better predict changes in future climate. Here we present a study of regionally calibrated winter (January) temperatures and according IWM intensities, based on a planktic foraminiferal record with biennial (2.55 years) resolution. Over the last ~250 years, IWM intensities gradually weakened, based on the long-term trend of reconstructed January temperatures. Furthermore, the results indicate that IWM is connected on interannual- to decadal time scales to climate variability of the tropical and extratropical Pacific, via El Niño Southern Oscillation and Pacific Decadal Oscillation. However, our findings suggest that this relationship appeared to begin to decouple since the beginning of the twentieth century. Cross-spectral analysis revealed that several distinct decadal-scale phases of colder climate and accordingly more intense winter monsoon centered at the years ~1800, ~1890 and ~1930 can be linked to changes of the North Atlantic Oscillation.

Keywords Indian winter monsoon · Mid-latitude climate interaction · El Niño Southern Oscillation · Pacific Decadal Oscillation · North Atlantic Oscillation

1 Introduction

The Indian monsoon, as the western branch of the Asian monsoon system, is the leading mode of seasonally changing temperature and precipitation in one of the world's most densely populated regions. During boreal winter, the winter monsoonal winds provide a connection of the high northern latitudes to the tropics, when cold air masses originating from the Siberian High are moving southwards (Wang et al. 2003, 2012). Western disturbances (WD) associated with the Indian winter monsoon (IWM) transport moisture from the Mediterranean to Central Asia and feed north Indian rivers and glaciers (Dimri et al. 2015 and references therein), contributing significantly to annual precipitation in the Himalaya region (Dimri 2013) and southern India (Bhanu Kumar et al. 2004). Moreover, winter temperatures in the Arabian Sea have shown to be related to the subsequent summer rainfall (Clark et al. 2000). To better understand how the monsoon system may change in response to future climate development, it is vital to study how monsoon climate changed through time and what underlying mechanisms are controlling it.

Palaeoclimatic studies of the Indian summer monsoon (ISM) showed that, apart from a dominant solar control

✉ Philipp M. Munz
philipp.munz@uni-tuebingen.de

[1] Department of Geosciences, Eberhard Karls Universität Tübingen, Hölderlinstr. 12, 72074 Tübingen, Germany

[2] Bundesanstalt für Geowissenschaften und Rohstoffe (BGR), Stilleweg 2, 30655 Hannover, Germany

[3] MARUM – Center for Marine Environmental Sciences, Leobener Str., 28359 Bremen, Germany

[4] Institute of Geology, University of Hamburg, Bundesstraße 55, 20146 Hamburg, Germany

[5] Leibniz Center for Tropical Marine Ecology, Fahrenheitstr. 6, 28359 Bremen, Germany

(Agnihotri et al. 2002; Gupta et al. 2005), variability of the ISM on millennial- and centennial timescales is likely linked to changes of North Atlantic climate (Böll et al. 2015), potentially through atmospherical reorganizations (Mohtadi et al. 2014). On decadal to interannual time scales, relationships between the North Atlantic Oscillation (NAO) and summer climate in Asia have been suggested (Liu and Yin 2001). There is abundant evidence that interannual- to decadal variability of the summer rainfall in India and East Asia is linked to tropical Indo-Pacific climate and modulated by perturbations of the Walker circulation associated with the state of El Niño Southern Oscillation (ENSO) (Webster et al. 1998; Terray et al. 2005; Krishna Kumar et al. 2006; Ashok and Saji 2007; Song and Zhou 2015), the phase of the Pacific Decadal Oscillation (PDO) (Krishnan and Sugi 2003; Krishnamurthy and Krishnamurthy 2014; Song and Zhou 2015), and the Indian Ocean Dipole (Ashok et al. 2004; Ummenhofer et al. 2013; Song and Zhou 2015). An intensification of the ENSO-summer monsoon relationship can be related to the phase of the PDO, where severe drought (flooding) is associated with the co-occurrence of El Niño (La Niña) with warm (cold) PDO modes. However, because of the strong impact of the summer season, proxy data of the winter monsoon are generally scarce and previously misinterpreted. Shen et al. (2013) for example showed for Lake Huguangyan, that Ti input and diagenetic conditions are controlled by vegetation density and therefore are, instead of East Asian winter monsoon, likely a function of summer precipitation. This demonstrates the need for long, quantitative high-resolution proxy data solely recording winter monsoon conditions, enabling to rigorously investigate internal and external forcing mechanisms.

During boreal winter, surface water hydrography in the northeastern Arabian Sea is associated with evaporative cooling, convective deepening of the mixed layer and entrainment of nutrients into the photic zone (Prasanna Kumar and Prasad 1999; Barber et al. 2001) induced by dry and cold northeasterly monsoonal winds. Planktic foraminifera are an especially valuable and widely used tool in paleoceanography (e.g. Kucera et al. 2005) reflecting trophic and thermal states of the upper water column by a variety of different proxies in the NE Arabian Sea (Schulz et al. 2002; Schiebel et al. 2004) with assemblage compositions primarily sensitive to winter sea-surface temperature (Munz et al. 2015). Here we present the first biennial resolution study of IWM intensity from a laminated

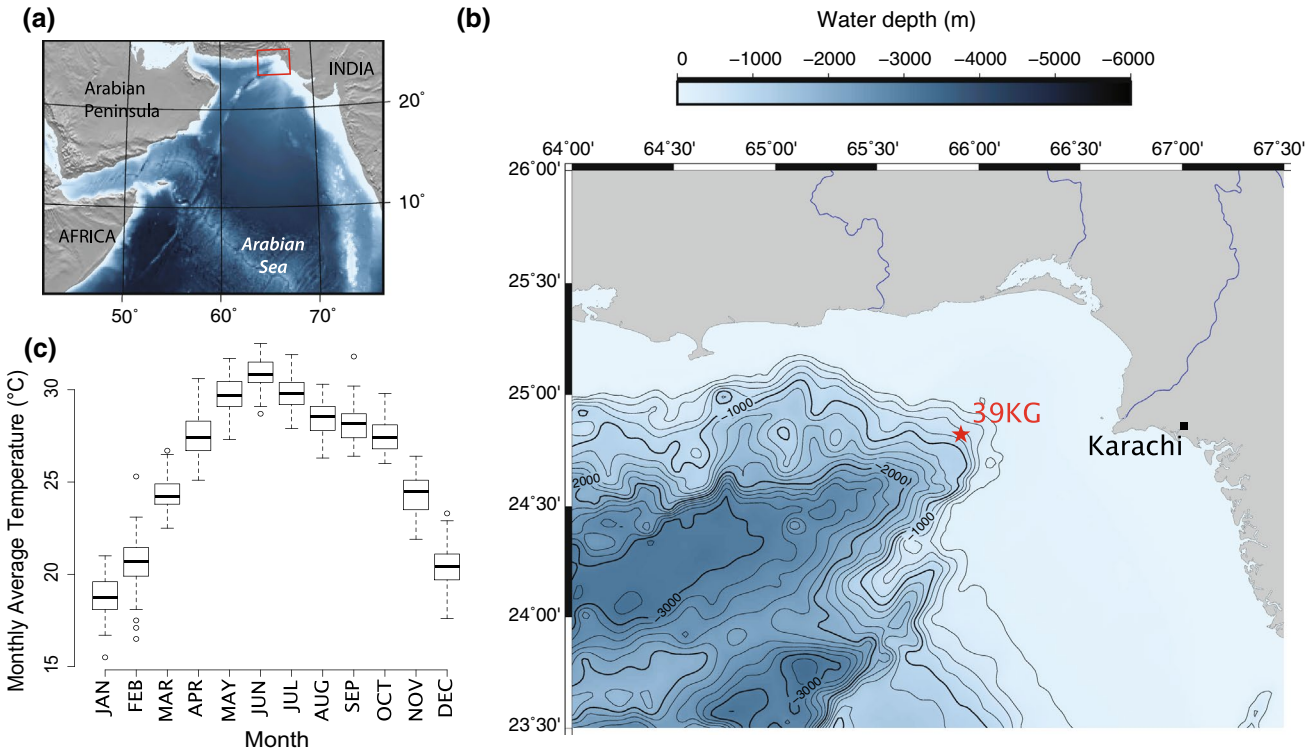

Fig. 1 **a**, **b** indicates the location of core SO90-39KG (N24° 49′ 18.599″; E65° 54′ 36″) in the northeastern Arabian Sea in 704 m water depth and ~160 nm west of Karachi. **c** Boxplot of monthly temperatures measured at Karachi weather stations (Karachi Manora and Karachi Airport, average where both stations are available) between 1878 and 1993 (data obtained from http://www.metoffice.gov.uk/research/climate/climate-monitoring/land-and-atmosphere/surface-station-records). January temperatures are continuously lowest during the annual cycle

marine sedimentary record off Pakistan (Fig. 1a, b) spanning the last ~250 years. During winter season, the region is under influence of northeasterly monsoonal winds that induce cold temperatures culminating in January (Fig. 1c). The winter temperature signals from PF assemblage compositions are first evaluated as the response to local winter temperatures from the instrumental temperature record. Reconstructed temperatures were then used to extend the record prior to 1850 into pre-industrial times to assess the evolution of IWM intensities and eventually identify significant long-term variability. This results in new evidence for the relationship of IWM with ENSO and PDO, which may have not been stable during the late Holocene but may have changed since the beginning of the twentieth century. However, decadal-scale episodes of intensive IWM may instead have been related to positive changes of NAO.

2 Materials and methods

2.1 Planktic foraminiferal record

Core 39KG was recovered on R/V SONNE's cruise SO90 in 1993 (von Rad et al. 1995) from the stable mid-depth oxygen minimum zone in 704 m water depth approximately 160 nm west of Karachi (Fig. 1b). Coarse fraction samples of a continuous 3-mm sampling scheme were available from a previous study (Doose-Rolinski et al. 2001). Determination of planktic foraminiferal assemblage compositions was described in Munz et al. (2015). We used a precise age control of absolute dates established from counting annual layers of the 'varve-like' laminated sediments (von Rad et al. 1999). The average age difference between the samples of core 39KG from the 3-mm resolution is 2.55 years.

To detect major trends in the PF faunal records, correspondence analysis (CA) was calculated with the statistical programming environment *R* ver. 3.2.1 (R Core Team 2015) and the package *vegan* ver. 2.3-1 (Oksanen et al. 2015). CA is a simple ordination method commonly used in ecology (Greenacre 2013), but unlike principal component analysis it preserves the Chi squared distance among the variables (e.g., Legendre and Birks 2012). CA was carried out on the raw counts of species having an overall relative abundance of >0.5%. 11 out of 20 species occurred in very low frequencies (<0.5%) and were excluded from further analyses to obtain a more robust signal-to-noise ratio (Kucera et al. 2005).

2.2 Observational and reanalysis data

Historical temperature data was obtained from the HadCRUT4 dataset infilled by kriging interpolation (Cowtan and Way 2014), the HadSST3.1.1.0 dataset (Kennedy et al. 2011) and the GISS Surface Temperature Analysis dataset GISTEMP (GISTEMP Team 2016). HadCRUT4 and GISTEMP are monthly observational datasets that combine sea surface temperature and land surface air temperature anomalies (Hansen et al. 2010, Morice et al. 2012) in order to cover regional winter climate of the area. The datasets cover the continuous period from 1850 (HadCRUT4) and 1880 (GISTEMP) to present. HadSST3.1.1.0, however, is a dataset of sea surface temperatures but has many data gaps prior to 1900. HadCRUT4 and HadSST3.1.1.0 are available on a 5° × 5° grid and monthly mean temperature anomalies from the three datasets were extracted from the grid cell containing the core location (20–25°N, 65–70°E). This area is to a large extent (80.4%) comprised of ocean surface in relation to land surface (19.6%). On a regional scale in the Arabian Sea, surface air temperatures and sea surface temperatures are shown to be highly correlated (Jaswal et al. 2012). Data were accessed through the KNMI climate explorer website (http://climexp.knmi.nl).

To enable a comparison of IWM with the East Asian winter monsoon (EAWM), two independent EAWM indices were calculated from the Twentieth Century Reanalysis dataset v2c (Compo et al. 2011), accurately reproducing EAWM conditions (Zhang et al. 2013). We used the index of Jhun and Lee (2004), defined as the area-averaged difference of the zonal wind at 300 hPa between the regions 27.5°–37.5°N, 110°–170°E and 50°–60°N, 80°–140°E, and the index of Chen et al. (2000), the meridional wind at 10 m of the regions 10°–25°N, 110°–130°E and 25°–40°N, 120°–140°E.

2.3 Data analysis and reconstructions

Winter temperature reconstructions were carried out using weighted-averaging-partial-least-squares (WA-PLS) regression and calibration (ter Braak and Juggins 1993) implemented in the package *rioja* (Juggins 2015) for *R*. WA-PLS is a common palaeoecological reconstruction method, as it combines several advantages compared to other methods (Birks et al. 2010). It is a combination of the WA regression and calibration technique, that models a unimodal species response and is based on the ecological niche concept, and PLS to extract the components (e.g., Juggins and Birks 2012). Biological abundance data was expressed as relative percentages of the nine most common species converted from raw counts. The selection criterion on model complexity was based on the respective minimum root mean squared error of prediction (RMSEP). Sample-specific errors of the reconstruction period and RMSEP were assessed via bootstrapping over 999 cycles.

Spectral analyses were performed using the multitaper method MTM (Mann and Lees 1996) with a red-noise null

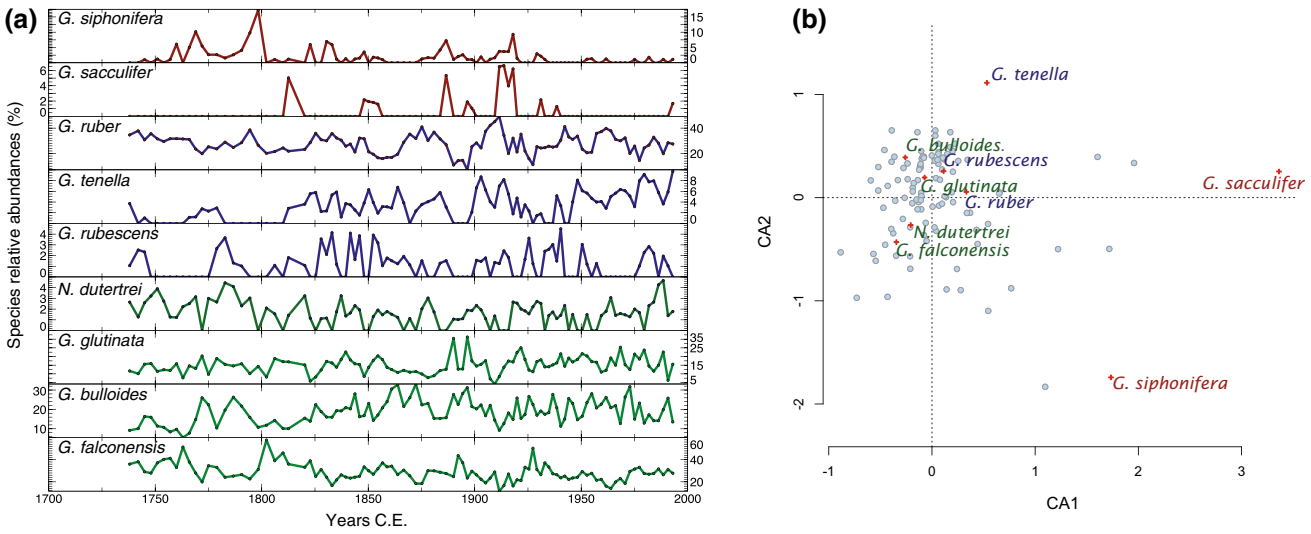

Fig. 2 **a** Relative frequencies of the nine species showing >0.5% average abundance that were used for further analyses. *Colours* indicate relative positioning along the first correspondence analysis axis in Fig. 2b. **b** Scatter bi-plot of the first and second correspondence analysis (CA) axes with sample (*blue dots*) and species (*red cross*) scores. Sample and site species scores are symmetrically scaled by the square root of their eigenvalues. The first axis explains 26.6% of the variance of the foraminiferal assemblage, the second axis 19.8%

hypothesis (Ghil 2002) implemented in the *SpectraWorks* software *kSpectra* ver. 3.4.5. Wavelet coherence analysis (Grinsted et al. 2004) was conducted with the MATLAB software and the package provided by Aslak Grinsted on the website http://noc.ac.uk/using-science/crosswavelet-wavelet-coherence. Time series were detrended and resampled to an equal-distant average spacing (2.55 yrs.) using piecewise cubic hermitean interpolation polynomials (PCHIP function of the *pracma* package ver. 1.6.4 for *R*) prior to MTM and wavelet coherence analyses.

For the calculation of linear correlation coefficients between two differently spaced time series, the records were binned along a new common time axis. The bin widths were chosen as the largest sample spacing within the respective period, with a 1-year overlap to either side.

2.4 Simulated temperature data

Monthly simulated January temperatures of climate model experiments were extracted from the 5° × 5° grid cell containing the core location (20–25°N; 65–70°E) from an ensemble of the Coupled Intercomparison Project 5 (http://cmip-pcmdi.llnl.gov/). Atmospheric and ocean output (Amon and Omon), as well as all available runs and model versions of the different models were averaged over the grid cell. Continuous time series were produced by combining results of each model from the last millennium (past 1000) and the historical experiments. Temperatures are expressed as anomalies relative to each model's average over the period 1700–1999.

3 Results

Over the entire record of core 39KG, the PF fauna of the nine species having a minimum average abundance of 0.5% (Fig. 2a) is dominated by *Globigerina falconensis* (29%) and *Globigerinoides ruber* (28%) followed by *Globigerina bulloides* (19%) and *Globigerinita glutinata* (15%). Minor abundances are shown by *Globoturborotalita tenella* (3.5%), *Globigerinella siphonifera* (2%), *Neogloboquadrina dutertrei* (2%), *Globoturborotalita rubescens* (1.5%) and *Globigerinoides sacculifer* (0.5%). An advantage of ordination methods like CA is the reduction of dimensionality of the original dataset to a lower number of synthetic variables, which explain as much of the variance of the original data as possible. The first and second CA axes together describe almost half (46.3%) of the information of the PF faunal dataset (Table 1). The first CA axis (CA1) separates *G. sacculifer* on the positive side from *G. falconensis* and *G. bulloides* on the negative side, whereas along the second axis (CA2) *G. tenella* is associated with positive and *G. siphonifera* with negative scores (Fig. 2b).

To identify any potential relationship between the PF faunal abundance data and historical temperature recordings, we regressed monthly temperature data from three observational datasets to CA1 and CA2 scores of samples overlapping with the temperature records. The sedimentary record of core 39KG accumulated on the sea floor over an average period of 2.55 ± 0.8 years, integrating the proxy signal of PF assemblages over this time span. A low-pass

Table 1 Eigenvalues and cumulative variance explained by the correspondence analysis based on nine species that showed an overall minimum abundance of 0.5%

	Eigenvalue	Cumulative variance explained (%)
CA1	0.047	26.6
CA2	0.035	46.3
CA3	0.030	63.3
CA4	0.023	76.3
CA5	0.016	85.3
CA6	0.013	92.7
CA7	0.009	97.7
CA8	0.004	100

filter was therefore applied to the monthly instrumental records with a 5-year cutoff frequency, to compensate for interannual variability during the proxy generation. From the monthly linear regression analyses of the three observational datasets with CA1 and CA2 scores (Fig. 3) we found that correlations are highest with January temperatures. This means that high (low) abundances of *G. falconensis* and *G. siphonifera* are related to colder (warmer) January temperatures and vice versa for *G. sacculifer* and *G. tenella*. This relationship of *G. falconensis* and *G. sacculifer* is in good agreement with a recent study (Munz et al. 2015), where we used redundancy analysis to characterize species response to environmental gradients with a surface sample dataset from the Arabian Sea. To discover the long-term temperature evolution and enable comparison with other calibrated proxy records we therefore used this relationship to reconstruct January temperatures prior to the instrumental period. Due to the longer overlap of the HadCRUT4 dataset with core 39KG and the good correlation with the planktic foraminiferal fauna (CA1: $r = 0.34$, $p = 0.006$; CA2: $r = 0.50$, $p < 0.0001$) it has given preference over the other records. Samples overlapping with the HadCRUT4 record (1852–1993, $n = 64$) were used for calibrating the transfer function by allocating the 5-year low-pass filtered temperature values to the respective samples of the foraminiferal record. $N = 36$ samples during 1738–1850 were used for reconstruction. A WA-PLS model with two components yielded the lowest prediction error (Table 2) and was chosen for quantitative reconstructions.

As long as monthly temperature measurements are available, January temperatures in Karachi are constantly recorded lowest during the annual cycle (Fig. 1c) and therefore leave a strong signal in the planktic foraminiferal fauna. Reconstructed temperatures are significantly correlated with CA

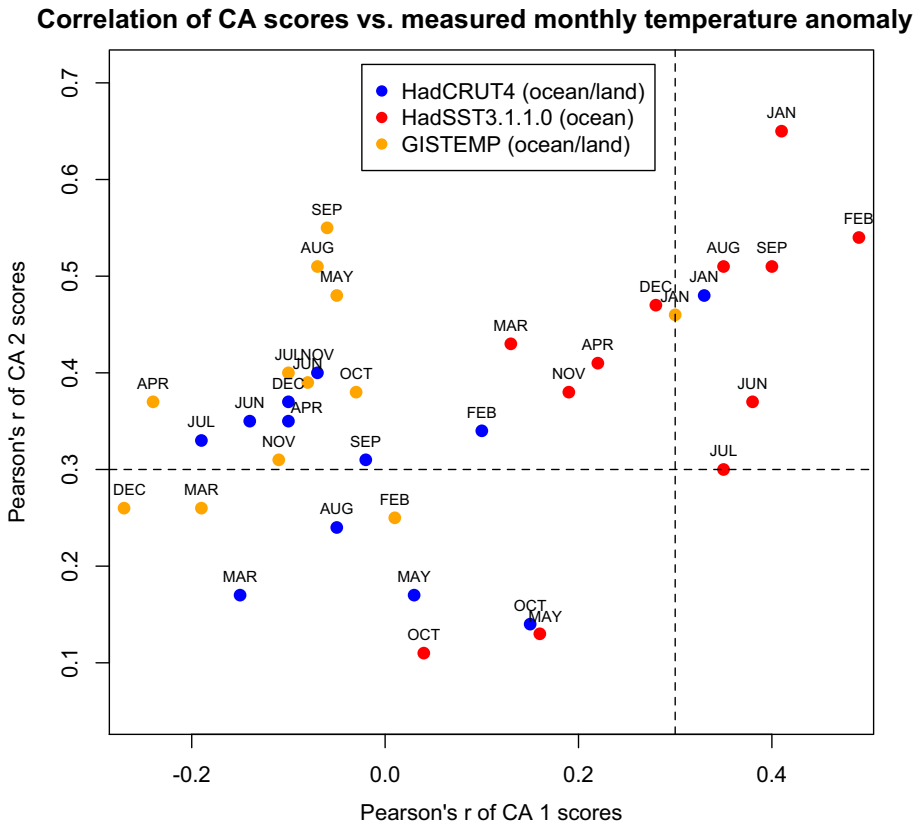

Fig. 3 Correlations of the first and second correspondence analysis (CA) scores of the planktic foraminiferal assemblages and the monthly temperatures from the HadCRUT4 (*blue dots*), HadSST3.1.1.0 (*red dots*) and GISTEMP (*orange dots*) datasets of the 5° × 5° grid cell containing the core station of core 39KG (20–25°N, 65–70°E). January temperatures from all three datasets showed highest positive correlation coefficients with CA1 and CA2 scores. Correlation coefficients of 0.3 are indicated by *dashed lines*

Table 2 Transfer function performance measures based on the root mean squared error (RMSE), the coefficients of determination and the cross-validated root mean squared error of prediction ($RMSEP_{boot}$)

	RMSE	Cross-val. R^2	$RMSEP_{boot}$
Component 1	0.340	0.222	0.372
Component 2	0.314	0.285	**0.366**
Component 3	0.310	0.291	0.367
Component 4	0.309	0.277	0.376
Component 5	0.309	0.268	0.382

Cross-validation is based on bootstrapping over 999 cycles. A transfer function model with two components yielded the lowest prediction error (highlighted)

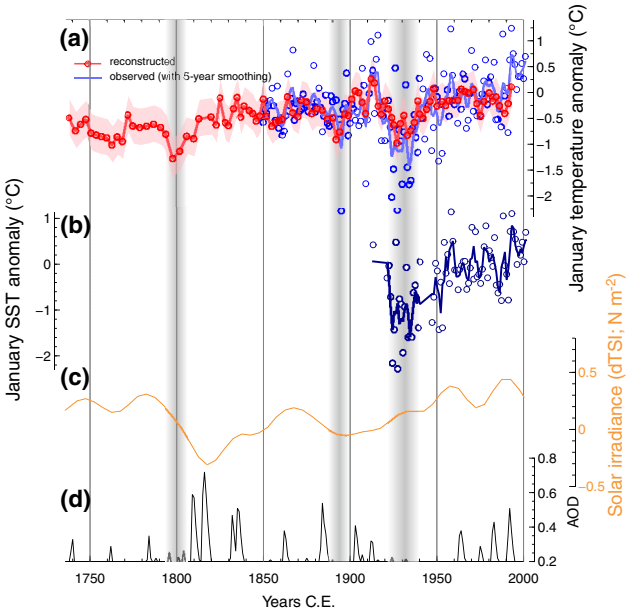

Fig. 4 **a** Reconstructed (*red line*) and observed (*blue circles*) January temperature anomalies. *Red shading* indicates reconstruction uncertainty based on bootstrapping (RMSEP). Observed temperatures were smoothed with a low-pass filter (5-year cutoff frequency) to compensate for high interannual variability (blue line). **b** January sea surface temperature (SST) anomaly of the area (20–25°N; 65–70°E) from the HadSST3.1.1.0 datatset, showing the same trend as integrated land/ocean temperatures in **a**. **c** Reconstructed solar irradiance of Steinhilber et al. (2009). **d** Reconstructed global volcanic aerosol optical depth (AOD) from Crowley and Unterman (2013). *Grey shaded vertical bars* indicate three decadal-scale cold episodes from the reconstructed and observed temperature records. *Black trend line* in **a** indicates a ~ 0.6 °C overall warming trend between 1738 and 1993

scores (CA1: $r = 0.28$, $p < 0.01$; CA2: $r = 0.88$, $p < 0.0001$), indicating that changes of the dominant foraminiferal taxa are primarily driven by the reconstructed temperatures (Juggins and Birks 2012). This is a valuable information, since the historical records contain measurements of surface temperatures (land surface, 0 m sea surface) and PF assemblages can potentially be more sensitive to sub-surface water conditions (Telford et al. 2013), which might then not be recording sea surface-atmosphere conditions correctly. The low-pass filtered instrumental temperatures plot generally within the uncertainty range of the reconstructions (Fig. 4) and both time series covary significantly (>99% confidence level) on sub-decadal to multi-decadal time scales (Fig. 5). This underlines that the foraminiferal-based reconstructions can be used as a valid tool to extend the historical record of regional winter temperature anomalies to pre-industrial times.

The record reveals three prominent decadal-scale episodes of very low temperatures, i.e. strong IWM intensities. The first, not covered by instrumental observations, from 1795 to 1805, as well as a second one from 1892 to 1894 and a third one from 1925 to 1935. Based on the calibrated relationship of the planktic foraminifera fauna and modern temperatures, the first and most severe cooling was −1.3 °C colder than the reference period (1961–1990), the second (−0.9 °C) and third (−1.0 °C) are almost equally intense. Reconstructed January temperatures were warmest in 1912 during the 'calibration period'. This warming was, however, unprecedented prior to 1850.

4 Discussion

4.1 Cold winter conditions and a potential relationship to incoming solar radiation

The first of the three cooling episodes shown in Fig. 4 falls together with the beginning of the Dalton solar minimum, lasting from 1780 to 1840 (Anet et al. 2014). Coldest temperatures, however, were recorded asynchronous and prior to periods of minimum irradiance forcing. Similar to basin-wide studies of tropical Indian Ocean springtime sea surface temperatures (Tierney et al. 2015) this may indicate, that solar irradiance is not the main driver of colder winter conditions.

Short-term anomalies of tropical (Tierney et al. 2015; Winter et al. 2015) and European (Sigl et al. 2015) summer climate was also affected by strong volcanic eruptions. Furthermore, volcanic eruptions led to an enhancement of the hydrological cycle in monsoonal Asia (Anchukaitis et al. 2010; Cui et al. 2014). Winter temperatures in Europe were anomalously warm in the years following large volcanic explosions (Robock and Mao 1992; Wegmann et al. 2014), while cold winter anomalies covered large parts of southern Asia (Shindell et al. 2004).

To test a potential short-lived response of winter conditions in our record to major volcanic eruptions, we compared timings of the four well documented major volcanic eruptions in the early nineteenth century (Schmidt et al. 2012), the two of unknown origin 1804 and 1809, the Tambora eruption in 1815, as well as two other tropical eruptions 1831 and 1835. None of those were apparently related to the first of

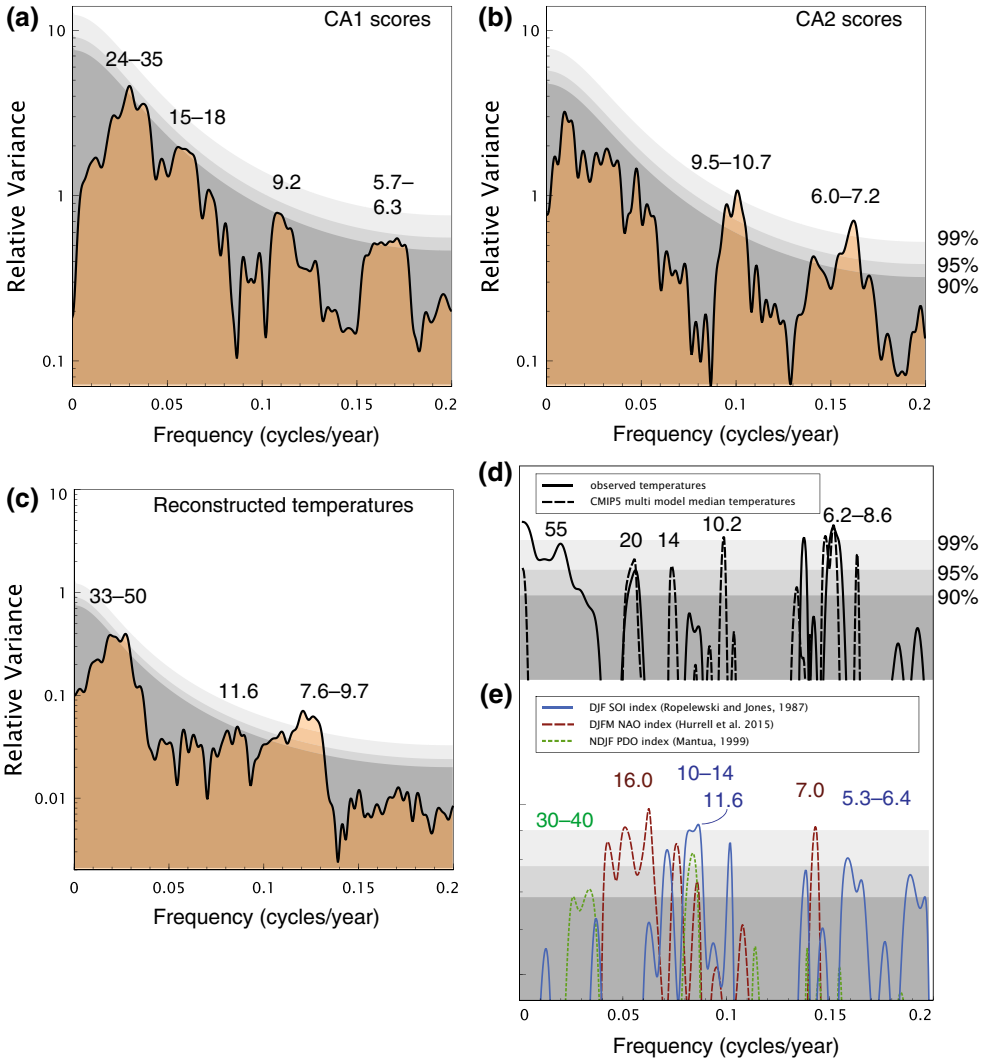

Fig. 5 Frequency spectra and coherence obtained with the multitaper method (MTM) using a red-noise null hypothesis (Ghil 2002). *Grey shading* indicates significance levels relative to the estimated red noise background above 90, 95 and 99%, respectively. MTM spectra and significant frequencies of CA1 scores **a**, CA2 scores **b** and the reconstructed January temperature anomalies **c**. Cross-power spectra and significantly coherent frequencies between reconstructed temperatures, as well as observed and simulated temperatures **d**, and respective circulation indices **e**

the noticeable three cold episodes, as volcanic eruptions and associated aerosol concentrations occurred ~5–30 years later (Fig. 4). The second cooling in the late nineteenth century occurred ~10 years after the Krakatoa eruption in 1883, while a possible response would be expected in the second year following the eruption (Shindell et al. 2004). Another smaller short-lived temperature anomaly in 1909, which is also evident from the instrumental temperature record, occurred 3 years earlier to the Novarupta/Katmai (Alaska) eruption in 1912. Generally, the temporal resolution of 2–3 years of our foraminiferal record could be below the detection limit needed to cover the short-lived response of atmospheric perturbations caused by major volcanic eruptions.

4.2 Teleconnections of IWM climate variability to large-scale circulation patterns

Reconstructed temperatures vary significantly on time scales between 7.6–9.7, 11.6 and 33–50 years (Fig. 5). These cycles are reflecting the periodicities of the planktic foraminiferal fauna, captured by CA1 and CA2 scores. Significant coherency of reconstructed temperatures with the observational-based Southern Oscillation index (SOI) was found on the 'classical' interannual ENSO bandwidth (5.3–6.4 years) and on a 11.6-year period (Fig. 5). Surprisingly, the ~12-year bandwidth also has coherencies with NAO and PDO indices, a cyclicity that was previously identified from tropical Atlantic trade wind intensity (Black et al. 1999) and Indian Ocean coral $\delta^{18}O$ (Charles et al. 1997; Cobb et al. 2001). This indicates that winter IWM intensities are modulated across seasons on decadal frequencies via a trans-regional teleconnection.

January temperatures are coherent with PDO indices on the 30–40-year cycle (Fig. 5) of PDO phase-shifts (Mantua et al. 1997). Thus, strong (weak) winter monsoon conditions follow cold (warm) PDO modes on decadal time scales. Warm January temperatures and accordingly weak IWM intensity apparently lags PDO warm

phases by several years (Fig. 6c, d). A cross-correlation analysis revealed a significant correlation ($r = 0.43$; $p < 0.05$) of reconstructed January temperatures and PDO 'warm modes' with a lag of ~8 years prior to 1940, which is also evident from phase arrows of a wavelet coherence analysis (Fig. 6f). Winter temperatures are lagging the anti-phase of SOI on the 10–14 year band by ~3 years (Fig. 6e), indicating that ENSO and PDO are modulating winter conditions, although on different frequency bands yet according to PDO modes. Within the interval 1900–1993, however, the correlation of January temperatures and PDO is not significant ($r = 0.18$; $p = 0.36$), indicating that the relationship of IWM and PDO is apparently weakening since the beginning of the twentieth century, several decades earlier than it was suggested for the relationship of ENSO and the Indian summer monsoon (Krishna Kumar et al. 1999).

NAO is, like ENSO, a major source of interannual global climate variability and contributes largely to Northern Hemisphere temperature patterns (Hurrell 1996). Reconstructed January temperatures and the reconstructed NAO index from Ortega et al. (2015) largely follow a common trend until ~1940 where both records diverge (Fig. 7a). Prior to 1940 both time series are highly correlated ($r = 0.62$; $p < 0.001$), after 1940 there is no linear dependence. Based on the finding that the close relationship to NAO is enhanced during the three distinct phases of colder climate (Fig. 7b), we hypothesize that the atmospheric circulation over the North Atlantic is the main driver for cold perturbations of IWM climate, potentially through an amplification of the Siberian High (Wu and Wang 2002).

These linkages, as well as the observed weakening of the PDO–IWM relationship and the general deficiency of describing ENSO and PDO properties in climate simulations (Bellenger et al. 2014) adds to the complexity of reproducing winter monsoon climatology in current state-of-the-art climate models (Gong et al. 2014). Although the simulated January temperatures are coherent with reconstructed and observed January temperatures on interdecadal- to decadal-scale frequencies (Fig. 5), models apparently fail to reproduce the timing and temperature pattern of our record (Fig. 8).

A noticeable feature of the record of reconstructed January temperatures is a long-term warming trend of ~+0.6 °C towards the present. Recent studies showed a rapid warming of winter temperatures by ~1.5 °C in India potentially associated with warming surface temperatures in the Arabian Sea (Alory et al. 2007; Kumar et al. 2009). A recent weakening of atmospheric winter climate conditions in Asia is supported by EAWM indices, which also indicate gradually decreasing EAWM intensities from ~1930

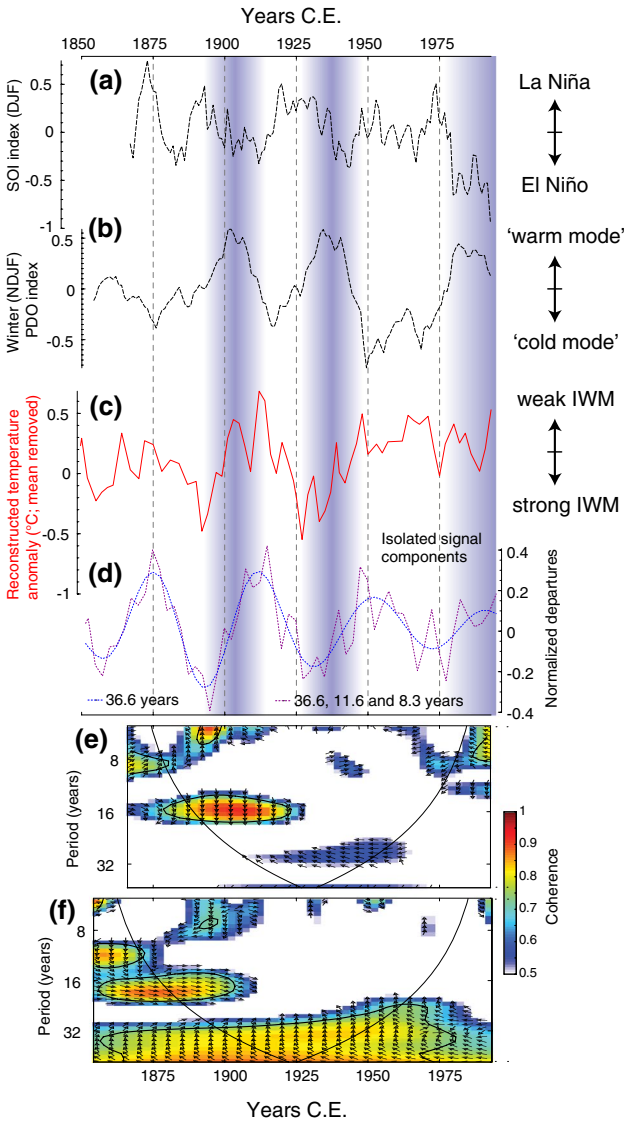

Fig. 6 Comparison of **a** winter (December–February) Southern Oscillation Index (SOI; 3-year running mean), **b** winter (November–February) Pacific Decadal Oscillation Index (PDO; 7-year running mean) and **c** detrended reconstructed January temperature anomaly of 39KG between 1850 and 1993. Vertical bars indicate apparent PDO 'warm phases'. **d** shows a reconstruction of the isolated signal components identified from the MTM spectrum in Fig. 5c as solely decadal (*blue stippling*) and summarised decadal- to inter-decadal components (*purple stippling*). Wavelet coherence analysis of reconstructed temperature estimates with winter (DJF) SOI (**e**) and (NDJF) PDO (**f**) indices. *Arrows* indicating phase relationships, i.e. for **e** *arrows pointing down* are interpreted as a 90° lag of January temperatures to the anti-phase of the winter SOI index. A 90° lag on a 10–14-year bandwidth would convert to 3 years. For **f** the *arrow pointing up* on the multidecadal ~36-year periodicity can be interpreted as PDO leading January temperatures by a 90° phase-angle, thus 90° at a wavelength of 36.6 years = 9.2 years. SOI is obtained from the NOAA Earth System Research Laboratory (http://www.esrl.noaa.gov/psd/gcos_wgsp/Timeseries/SOI/), PDO from http://www.ncdc.noaa.gov/teleconnections/pdo/

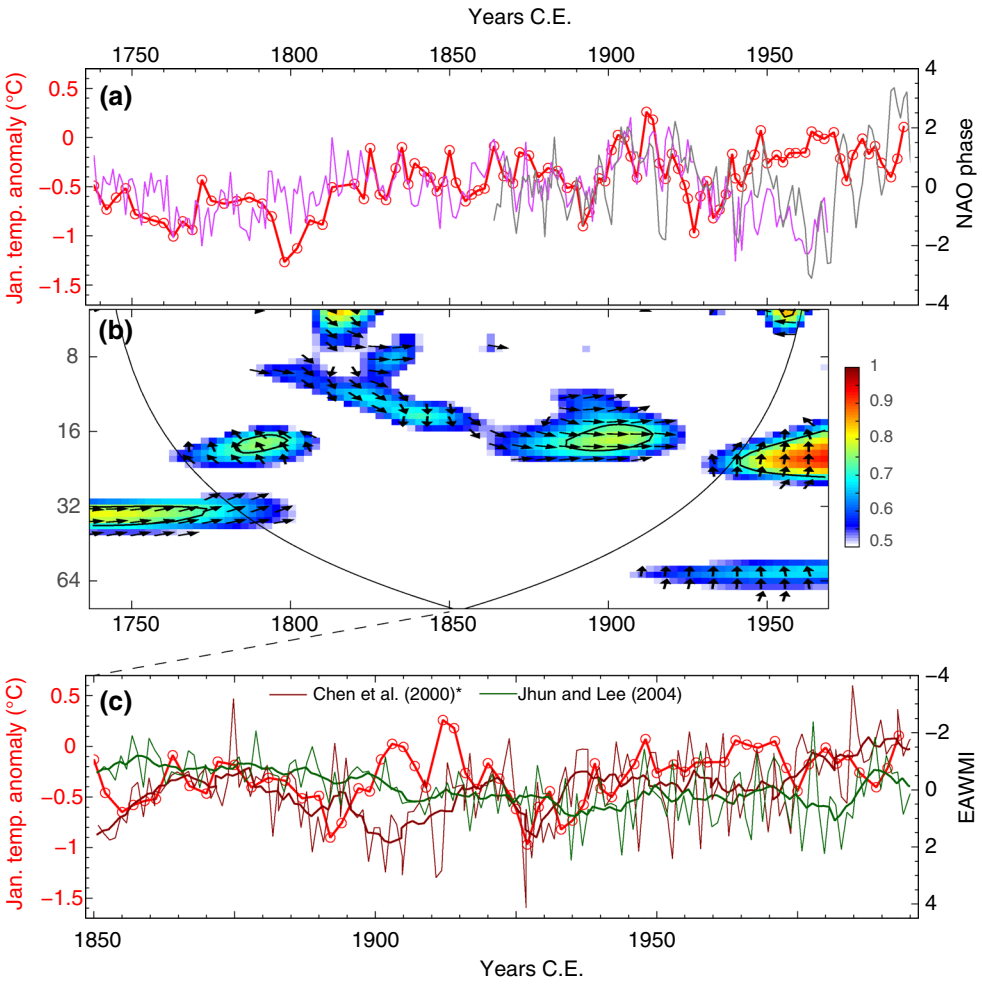

Fig. 7 **a** Time series of the reconstructed January temperature anomalies (*red line*) with the reconstructed model-constrained North Atlantic Oscillation (NAO_{mc}, *purple line*) from Ortega et al. (2015) and the winter (DJFM) instrumental NAO index (*grey line*, Hurrell 1995). **b** Wavelet coherence analysis reveals that both records show highest coherency around the three obvious cold spells of the winter temperature record. Coherency on the 16-year bandwidth is consistent with the instrumental-based winter NAO index (Fig. 5e). **c** Reconstructed January temperatures (*red*) with East Asian Winter Monsoon indices (EAWMI) calculated from reanalysis data. Thin lines are original data, thick lines are 7-pt moving averages. The index of Chen et al. (2000) has been multiplied by −1 with respect to the original definition (*star*) so that positive values of both indices correspond to strong EAWM. Please note the reversed scaling to facilitate direct comparison

towards the present (Fig. 7c). This indicates that winter monsoon intensity, reflected by January temperatures, is gradually weakening towards the present and that this trend is associated with a decrease of the atmospheric winter monsoon circulation.

It seems likely that the continuing attenuation of IWM intensity, even after the teleconnections with PDO and NAO are weakening, is associated with the recent global warming trend. IWM circulation is strongly associated with surface air temperature fluctuations in the high northern latitudes. It has been shown by several studies (Wang and Gaffen 2001; Liu et al. 2004) that surface air temperatures in northern China, especially winter temperatures, experienced a significant increase since the middle of the twentieth century. A continental-scale warming of Eurasian surface temperatures induced a pronounced weakening of the intensity of the Siberian High (Gong and Ho 2002), attenuating the large-scale meridional temperature gradient and the northerly winter winds (Hu et al. 2000; Hori and Ueda 2006).

The apparent decoupling of IWM intensity from global-scale teleconnections is an important finding in the context of a possible future development of winter precipitation brought by WD, synoptic-scale cyclonic storms associated with the westerlies during winter (reviewed by Dimri et al. 2015). WD are coupled to IWM intensity through increased convective activity in the middle to upper troposphere and a southward shift of the mid-latitude Subtropical Westerly Jet. Perturbation of IWM circulation thus likely influences the activity and frequency of WD formation. A recent warming of the mid-troposphere over the Tibetan Plateau has increased the regional baroclinicity, which led to higher variability and more extreme winter precipitation events (Madhura et al. 2014). However, the temporal and spatial pattern of WD precipitation over the Himalayan region is complex and requires further investigation (Dimri et al. 2015).

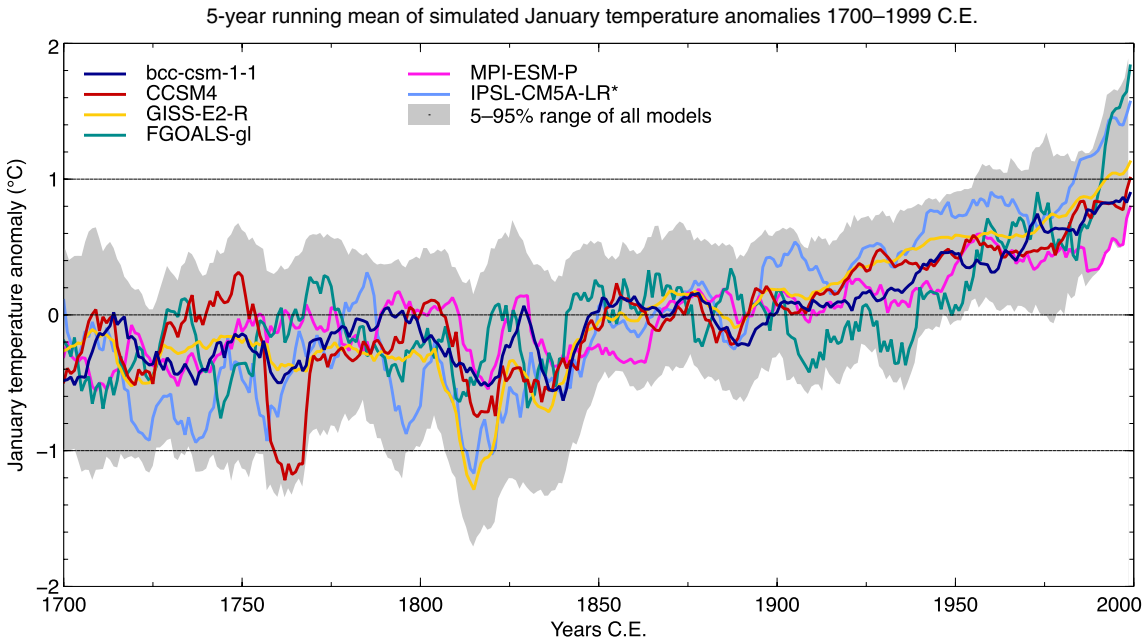

Fig. 8 Simulated January temperature anomalies (relative to the each model's average from 1700 to 1999 and smoothed with a 5-year running average) obtained from the Coupled Model Intercomparison Project 5 of the grid cell containing the core location of 39KG (20–25°N; 65–70°E) covering the period 1700–1999. The 5%–95% percentile ranges of all models are plotted as *grey shading*. Results of the IPSL-CM5A-LR experiment (*star*) does only contain atmospheric output (*Amon*)

5 Summary

Our results show that winter monsoon intensities in the Arabian Sea are coupled to Pacific and North Atlantic climate, but with a complex and shifting pattern. A better understanding of extratropical and tropical influences on winter monsoon climate might help to improve model performance (Levine et al. 2013), and hence, predictability of tropical to mid-latitude winter climate conditions in the Northern Hemisphere.

Acknowledgements The study was supported by the German Ministry of Education and Research (BMBF) as part of the project CARIMA (Grant No. 03G0806C). R. Krishnan made general comments on the topic, which is highly appreciated. Support for the Twentieth Century Reanalysis Project dataset is provided by the U.S. Department of Energy, Office of Science Innovative and Novel Computational Impact on Theory and Experiment (DOE INCITE) program, and Office of Biological and Environmental Research (BER), and by the National Oceanic and Atmospheric Administration Climate Program Office. We thank two anonymous reviewers for their constructive comments that helped to improve the manuscript. The planktic foraminiferal assemblage data and reconstruction results of January temperatures are available electronically at the PANGAEA Data Publisher for Earth & Environmental Science (https://doi.pangaea.de/10.1594/PANGAEA.866924).

References

Agnihotri R, Dutta K, Bhushan R, Somayajulu B (2002) Evidence for solar forcing on the Indian monsoon during the last millennium. Earth Planet Sci Lett 198:521–527. doi:10.1016/S0012-821X(02)00530-7

Alory G, Wijffels S, Meyers G (2007) Observed temperature trends in the Indian Ocean over 1960–1999 and associated mechanisms. Geophys Res Lett 34:L02606. doi:10.1029/2006GL028044

Anchukaitis KJ, Buckley BM, Cook ER et al (2010) Influence of volcanic eruptions on the climate of the Asian monsoon region. Geophys Res Lett. doi:10.1029/2010GL044843

Anet JG, Muthers S, Rozanov EV et al (2014) Impact of solar versus volcanic activity variations on tropospheric temperatures and precipitation during the Dalton Minimum. Clim Past 10:921–938. doi:10.5194/cp-10-921-2014

Ashok K, Saji NH (2007) On the impacts of ENSO and Indian Ocean dipole events on sub-regional Indian summer monsoon rainfall. Nat Hazards 42:273–285. doi:10.1007/S11069-006-9091-0

Ashok K, Guan Z, Saji NH, Yamagata T (2004) Individual and combined influences of ENSO and the Indian Ocean dipole on the Indian summer monsoon. J Clim. doi:10.1175/1520-0442(2004)017<3141:IACIOE>2.0.CO;2

Barber RT, Marra J, Bidigare RC et al (2001) Primary productivity and its regulation in the Arabian Sea during 1995. Deep-Sea Res II 48:1127–1172. doi:10.1016/S0967-0645(00)00134-X

Bellenger H, Guilyardi E, Leloup J et al (2014) ENSO representation in climate models: from CMIP3 to CMIP5. Clim Dyn 42:1999–2018. doi:10.1007/s00382-013-1783-z

Bhanu Kumar OSRU, Kumar OSRUB, Naidu CV et al (2004) Prediction of southern Indian winter monsoon rainfall from September local upper-air temperatures. Meteorol Appl 11:189–199. doi:10.1017/S1350482704001306

Birks H, Heiri O, Seppä H, Bjune AE (2010) Strengths and weaknesses of quantitative climate reconstructions based on late-quaternary biological proxies. Open Ecol J 3:68–110

Black DE, Peterson LC, Overpeck JT et al (1999) Eight centuries of North Atlantic Ocean atmosphere variability. Science 286:1709–1713. doi:10.1126/science.286.5445.1709

Böll A, Schulz H, Munz PM et al (2015) Contrasting sea surface temperature of summer and winter monsoon variability in the northern Arabian Sea over the last 25 ka. Palaeogeogr Palaeoclimatol Palaeoecol 426:10–21. doi:10.1016/j.palaeo.2015.02.036

Charles CD, Hunter DE, Fairbanks RG (1997) Interaction between the ENSO and the Asian monsoon in a coral record of tropical climate. Science 277:925–928. doi:10.1126/science.277.5328.925

Chen W, Graf HF, Huang RH (2000) The interannual variability of East Asian winter monsoon and its relation to the summer monsoon. Adv Atmos Sci 17:46–60

Clark CO, Cole JE, Webster PJ (2000) Indian Ocean SST and Indian summer rainfall: predictive relationships and their decadal variability. J Clim. doi:10.1175/1520-0442(2000)013<2503:IOSAIS>2.0.CO;2

Cobb KM, Charles CD, Hunter DE (2001) A central tropical Pacific coral demonstrates Pacific, Indian, and Atlantic decadal climate connections. Geophys Res Lett 28:2209–2212. doi:10.1029/2001GL012919

Compo GP, Whitaker JS, Sardeshmukh PD, Matsui N, Allan RJ et al (2011) The twentieth century reanalysis project. Q J R Meteorol Soc 137:1–28. doi:10.1002/qj.776

Cowtan K, Way RG (2014) Coverage bias in the HadCRUT4 temperature series and its impact on recent temperature trends. Q J R Meteorol Soc 140:1935–1944. doi:10.1002/qj.2297

Crowley TJ, Unterman MB (2013) Technical details concerning development of a 1200 yr proxy index for global volcanism. Earth Syst Sci Data 5:187–197. doi:10.5194/essd-5-187-2013

Cui X, Gao Y, Sun J (2014) The response of the East Asian summer monsoon to strong tropical volcanic eruptions. Adv Atmos Sci 31:1245–1255. doi:10.1007/s00376-014-3239-8

Dimri AP (2013) Intraseasonal oscillation associated with the Indian winter monsoon. J Geophys Res Atmos 118:1189–1198. doi:10.1002/jgrd.50144

Dimri AP, Niyogi D, Barros AP et al (2015) Western disturbances: a review. Rev Geophys 53:225–246. doi:10.1002/2014RG000460

Doose-Rolinski H, Rogalla U, Scheeder G et al (2001) High-resolution temperature and evaporation changes during the late Holocene in the northeastern Arabian Sea. Paleoceanography 16:358–367

Ghil M (2002) Advanced spectral methods for climatic time series. Rev Geophys 40:1003. doi:10.1029/2000RG000092

GISTEMP Team (2016) GISS Surface Temperature Analysis (GISTEMP). NASA Goddard Institute for Space Studies. Dataset accessed 2016-07-15 at http://data.giss.nasa.gov/gistemp/

Gong DY, Ho CH (2002) The Siberian high and climate change over middle to high latitude Asia. Theor Appl Climatol 72:1–9. doi:10.1007/s007040200008

Gong H, Wang L, Chen W et al (2014) The climatology and interannual variability of the East Asian winter monsoon in CMIP5 models. J Clim 27:1659–1678. doi:10.1175/JCLI-D-13-00039.1

Greenacre M (2013) The contributions of rare objects in correspondence analysis. Ecology 94:241–249. doi:10.1890/11-1730.1

Grinsted A, Moore JC, Jevrejeva S (2004) Application of the cross wavelet transform and wavelet coherence to geophysical time series. Nonlinear Process Geophys 11:561–566. doi:10.5194/npg-11-561-2004

Gupta AK, Das M, Anderson DM (2005) Solar influence on the Indian summer monsoon during the Holocene. Geophys Res Lett 32:L17703. doi:10.1029/2005GL022685

Hansen J, Ruedy R, Sato M, Lo K (2010) Global surface temperature change. Rev Geophys 48:RG4004. doi:10.1029/2010RG000345

Hori ME, Ueda H (2006) Impact of global warming on the East Asian winter monsoon as revealed by nine coupled atmosphere-ocean GCMs. Geophys Res Lett 33:L03713–L03714. doi:10.1029/2005GL024961

Hu Z-Z, Bengtsson L, Arpe K (2000) Impact of global warming on the Asian winter monsoon in a coupled GCM. J Geophys Res 105:4607–4624. doi:10.1029/1999JD901031

Hurrell JW (1995) Decadal trends in the North Atlantic Oscillation and relationships to regional temperature and precipitation. Science 269:676–679. doi:10.1126/science.269.5224.676

Hurrell JW (1996) Influence of variations in extratropical wintertime teleconnections on northern hemisphere temperature. Geophys Res Lett 23:665–668. doi:10.1029/96GL00459

Jaswal AK, Singh V, Bhambak SR (2012) Relationship between sea surface temperature and surface air temperature over Arabian Sea, Bay of Bengal and Indian Ocean. J Ind Geophys Union 16(2):41–53

Jhun JG, Lee EJ (2004) A new East Asian winter monsoon index and associated characteristics of the winter monsoon. J Clim 17:711–726

Juggins S (2015) rioja: analysis of quaternary science data. R package version 0.9-5, http://cran.r-project.org/package=rioja

Juggins S, Birks HJB (2012) Quantitative environmental reconstructions from biological data. In: Birks HJB, Lotter AF, Juggins S, Smol JP (eds) Tracking environmental change using lake sediments. Data handling and statistical techniques, vol 5. Springer, Dordrecht, pp 431–494

Kennedy JJ, Rayner NA, Smith RO, Saunby M, Parker DE (2011) Reassessing biases and other uncertainties in sea-surface temperature observations since 1850 part 1: measurement and sampling errors. J Geophys Res 116:D14103. doi:10.1029/2010JD015218

Krishna Kumar K, Rajagopalan B, Cane M (1999) On the weakening relationship between the Indian monsoon and ENSO. Science 284:2156–2159. doi:10.1126/science.284.5423.2156

Krishna Kumar K, Rajagopalan B, Hoerling M et al (2006) Unraveling the mystery of Indian monsoon failure during El Niño. Science 314:115–119. doi:10.1126/science.1131152

Krishnamurthy L, Krishnamurthy V (2014) Decadal scale oscillations and trend in the Indian monsoon rainfall. Clim Dyn 43:319–331. doi:10.1007/s00382-013-1870-1

Krishnan R, Sugi M (2003) Pacific decadal oscillation and variability of the Indian summer monsoon rainfall. Clim Dyn 21:233–242. doi:10.1007/s00382-003-0330-8

Kucera M, Weinelt M, Kiefer T et al (2005) Reconstruction of sea-surface temperatures from assemblages of planktonic foraminifera: multi-technique approach based on geographically constrained calibration data sets and its application to glacial Atlantic and Pacific Oceans. Quat Sci Rev 24:951–998. doi:10.1016/j.quascirev.2004.07.014

Kumar SP, Roshin RP, Narvekar J, Kumar PK, Vivekanandan E (2009) Response of the Arabian Sea to global warming and associated regional climate shift. Mar Environ Res 68(5):217–222. doi:10.1016/j.marenvres.2009.06.010

Legendre P, Birks HJB (2012) Chapter 8: From classical to canonical ordination. In: Birks HJB, Lotter AF, Juggins S, Smol JP (eds) Tracking environmental change using lake sediments. Data handling and numerical techniques, vol 5. Springer, Dordrecht, pp 201–248

Levine RC, Turner AG, Marathayil D, Martin GM (2013) The role of northern Arabian Sea surface temperature biases in CMIP5 model simulations and future projections of Indian summer monsoon rainfall. Clim Dyn 41:155–172. doi:10.1007/s00382-012-1656-x

Liu X, Yin Z-Y (2001) Spatial and temporal variation of summer precipitation over the Eastern Tibetan Plateau and the North Atlantic Oscillation. J Clim 14:2896–2909. doi:10.1175/1520-0442(2001)014<2896:SATVOS>2.0.CO;2

Liu B, Xu M, Henderson M et al (2004) Taking China's temperature: daily range, warming trends, and regional variations, 1955–2000. J Clim 17:4453–4462. doi:10.1175/3230.1

Madhura RK, Krishnan R, Revadekar JV et al (2014) Changes in western disturbances over the Western Himalayas in a warming environment. Clim Dyn 44:1157–1168. doi:10.1007/s00382-014-2166-9

Mann ME, Lees JM (1996) Robust estimation of background noise and signal detection in climatic time series. Clim Chang 33:409–445. doi:10.1007/BF00142586

Mantua NJ, Hare SR, Zhang Y et al (1997) A Pacific decadal climate oscillation with impacts on salmon production. Bull Am Meteorol Soc 78:1069–1079. doi:10.1175/1520-0477(1997)078<1069:APICOW>2.0.CO;2

Mohtadi M, Prange M, Oppo DW et al (2014) North Atlantic forcing of tropical Indian Ocean climate. Nature 509:76–80. doi:10.1038/nature13196

Morice CP, Kennedy JJ, Rayner NA, Jones PD (2012) Quantifying uncertainties in global and regional temperature change using an ensemble of observational estimates: the HadCRUT4 data set. J Geophys Res 117:D08101. doi:10.1029/2011JD017187

Munz PM, Siccha M, Lückge A et al (2015) Decadal-resolution record of winter monsoon intensity over the last two millennia from planktic foraminiferal assemblages in the northeastern Arabian Sea. Holocene 25:1756–1771. doi:10.1177/0959683615591357

Oksanen J, Blanchet FG, Kindt R et al (2015) vegan: community ecology package. R package version 2.3-1, http://cran.r-project.org/package=vegan

Ortega P, Lehner F, Swingedouw D et al (2015) A model-tested North Atlantic Oscillation reconstruction for the past millennium. Nature 523:71–74. doi:10.1038/nature14518

Prasanna Kumar S, Prasad TG (1999) Formation and spreading of Arabian Sea high-salinity water mass. J Geophys Res 104:1455–1464. doi:10.1029/1998JC900022

Robock A, Mao J (1992) Winter warming from large volcanic eruptions. Geophys Res Lett 19:2405–2408. doi:10.1029/92GL02627

Schiebel R, Zeltner A, Treppke UF, Waniek JJ (2004) Distribution of diatoms, coccolithophores and planktic foraminifers along a trophic gradient during SW monsoon in the Arabian Sea. Mar Micropaleontol 51:345–371. doi:10.1016/j.marmicro.2004.02.001

Schmidt A, Carslaw KS, Mann GW et al (2012) Importance of tropospheric volcanic aerosol for indirect radiative forcing of climate. Atmos Chem Phys 12:7321–7339. doi:10.5194/acp-12-7321-2012

Schulz H, von Rad U, Ittekkot V (2002) Planktic foraminifera, particle flux and oceanic productivity off Pakistan, NE Arabian Sea: modern analogues and application to the palaeoclimatic record. In: Clift PD, Kroon D, Gaedicke C, Craig J (eds) The tectonic and climatic evolution of the Arabian Sea region. Geological Society of London, Special Publication 195, London, pp 499–516

Shen J, Wu X, Zhang Z et al (2013) Ti content in Huguangyan maar lake sediment as a proxy for monsoon-induced vegetation density in the Holocene. Geophys Res Lett 40:5757–5763. doi:10.1002/grl.50740

Shindell DT, Schmidt GA, Mann ME, Faluvegi G (2004) Dynamic winter climate response to large tropical volcanic eruptions since 1600. J Geophys Res 109:D05104. doi:10.1029/2003JD004151

Sigl M, Winstrup M, McConnell JR et al (2015) Timing and climate forcing of volcanic eruptions for the past 2,500 years. Nature 523:543–549. doi:10.1038/nature14565

Song F, Zhou T (2015) The crucial role of internal variability in modulating the decadal variation of the East Asian Summer Monsoon–ENSO relationship during the twentieth century. J Clim 28:7093–7107. doi:10.1175/JCLI-D-14-00783.1

Steinhilber F, Beer J, Fröhlich C (2009) Total solar irradiance during the Holocene. Geophys Res Lett 36:L19704. doi:10.1029/2009GL040142

R Core Team (2015) R: a language and environment for statistical computing. R Foundation for statistical computing, Vienna, Austria. http://www.R-project.org

Telford RJ, Li C, Kucera M (2013) Mismatch between the depth habitat of planktonic foraminifera and the calibration depth of SST transfer functions may bias reconstructions. Clim Past 9:859–870. doi:10.5194/cp-9-859-2013

ter Braak CJF, Juggins S (1993) Weighted averaging partial least squares regression (WA-PLS): an improved method for reconstructing environmental variables from species assemblages. Hydrobiologia 269–270:485–502

Terray P, Guilyardi E, Fischer AS, Delecluse P (2005) Dynamics of the Indian monsoon and ENSO relationships in the SINTEX global coupled model. Clim Dyn 24:145–168. doi:10.1007/s00382-004-0479-9

Tierney JE, Abram NJ, Anchukaitis KJ et al (2015) Tropical sea surface temperatures for the past four centuries reconstructed from coral archives. Paleoceanography 30:226–252. doi:10.1002/2014PA002717

Ummenhofer CC, Ummenhofer C, D'Arrigo R et al (2013) Links between Indo-Pacific climate variability and drought in the Monsoon Asia Drought Atlas. Clim Dyn 40:1319–1334. doi:10.1007/s00382-012-1458-1

von Rad U, Schulz H, Erlenkeuser H et al (1995) Sampling the oxygen minimum zone off Pakistan: glacial-interglacial variations of anoxia and productivity (preliminary results, SONNE 90 cruise). Mar Geol 125:7–19. doi:10.1016/0025-3227(95)00051-Y

von Rad U, Schaaf M, Michels KH et al (1999) A 5000-yr record of climate change in varved sediments from the oxygen minimum zone off Pakistan, northeastern Arabian sea. Quatern Res 51:39–53. doi:10.1006/qres.1998.2016

Wang JXL, Gaffen DJ (2001) Late-twentieth-century climatology and trends of surface humidity and temperature in China. J Clim 14:2833–2845. doi:10.1175/1520-0442(2001)014<2833:ltccat>2.0.co;2

Wang B, Clemens SC, Liu P (2003) Contrasting the Indian and East Asian monsoons: implications on geologic timescales. Mar Geol 201:5–21. doi:10.1016/S0025-3227(03)00196-8

Wang L, Li J, Lu H et al (2012) The East Asian winter monsoon over the last 15,000 years: its links to high-latitudes and tropical climate systems and complex correlation to the summer monsoon. Quat Sci Rev 32:131–142. doi:10.1016/j.quascirev.2011.11.003

Webster PJ, Magaña VO, Palmer TN et al (1998) Monsoons: processes, predictability, and the prospects for prediction. J Geophys Res Oceans 103:14451–14510

Wegmann M, Brönnimann S, Bhend J et al (2014) Volcanic influence on european summer precipitation through monsoons: possible cause for "Years without Summer". J Clim 27:3683–3691. doi:10.1175/JCLI-D-13-00524.1

Winter A, Zanchettin D, Miller T et al (2015) Persistent drying in the tropics linked to natural forcing. Nat Commun 6:7627. doi:10.1038/ncomms8627

Wu B, Wang J (2002) Winter Arctic Oscillation, Siberian high and East Asian winter monsoon. Geophys Res Lett 29:1897. doi:10.1029/2002GL015373

Zhang ZY, Guo WL, Gong DY, Kim S-J (2013) Evaluation of the twentieth century reanalysis dataset in describing East Asian winter monsoon variability. Adv Atmos Sci 30(6):1645–1652. doi:10.1007/s00376-012-2226-1